frontiers in Chemical Engineering

ORIGINAL RESEARCH
published: 12 January 2022
doi: 10.3389/fceng.2021.764931

Synthesis and Characterization of NiMo Catalysts Supported on Fine Carbon Particles for Hydrotreating: Effects of Metal Loadings in Catalyst Formulation

Emma Aryee[1], *Ajay Kumar Dalai*[1]* *and John Adjaye*[2]

[1]Catalysis and Chemical Reaction Engineering Laboratories, Department of Chemical Engineering, University of Saskatchewan, Saskatoon, SK, Canada, [2]Syncrude Edmonton Research Centre, Edmonton, AB, Canada

The by-products collected during the synthesis of carbon nanohorns via the arc discharge synthesis method is comprised of other carbon particles (OCP). At a hydrotreating operating temperature of 370°C, preliminary investigations using a bimetallic catalyst with support originating from the fine fractions of other carbon particles (OCP_f) and containing 13 wt% Mo and 2.5 wt% Ni resulted in an HDS and HDN conversion of 78 and 25%, respectively. Variation of metal compositions in catalyst formulation and its impact on hydrotreating activity was therefore considered in this study to enhance the hydrotreating activity of OCP_f–supported catalyst, and to determine if the best NiMo/OCP_f catalyst achieved from this study could be a viable catalyst for hydrotreating applications. The co-incipient wetness impregnation was used in preparing series of hydrotreating catalysts with Ni and Mo loadings within the range of (2.5–5.0 wt%) and (13–26 wt%) respectively. Overall, the catalyst samples with maximum Ni loading of 5.0 wt% and Mo loadings of either 13 or 19 wt% showed higher dispersion and the ability to form a Type II Ni-Mo-S phase with enhanced activity. The effects of metal compositions on both HDS and HDN activities were correlated with their physicochemical properties.

Keywords: carbon-supported catalysts, arc discharge, by-products, metal compositions, type II Ni-Mo-S phase, hydrodesulfurization, hydrodenitrogenation, characterizations

OPEN ACCESS

Edited by:
Jose Escobar,
Mexican Institute of Petroleum, Mexico

Reviewed by:
Mohan Rana,
Kuwait Institute for Scientific Research, Kuwait
Luděk Kaluža,
Institute of Chemical Process Fundamentals (ASCR), Czechia

***Correspondence:**
Ajay Kumar Dalai
ajay.dalai@usask.ca

Specialty section:
This article was submitted to Catalytic Engineering, a section of the journal Frontiers in Chemical Engineering

Received: *26 August 2021*
Accepted: *10 December 2021*
Published: *12 January 2022*

Citation:
Aryee E, Dalai AK and Adjaye J (2022) Synthesis and Characterization of NiMo Catalysts Supported on Fine Carbon Particles for Hydrotreating: Effects of Metal Loadings in Catalyst Formulation. Front. Chem. Eng. 3:764931. doi: 10.3389/fceng.2021.764931

INTRODUCTION

Hydrotreating is a catalytic hydrogenation process that is globally used to upgrade highly contaminated crude oil into high quality products with reduced sulfur, nitrogen, oxygen, and metal content. The hydrotreating process also leads to the conversion of aromatics and olefins in the crude oil into saturated products. Hydrotreating therefore helps to meet the demands for cleaner environment and stricter regulations. Since this process is catalytically driven, development of a hydrotreating catalyst is one way of achieving optimal hydrotreating effect. Apart from the support other key components of the catalyst are the active metals and promoters. Commonly used hydrotreating catalysts are supported-CoMo and -NiMo sulfides, and typical metal loading compositions for Ni (Co) and Mo are within the range of (3–8 wt%) and (10–30 wt%), respectively (Robinson and Dolbear, 2006; Jarullah et al., 2012).

For a hydrotreating catalyst such as $NiMo/Al_2O_3$ the main catalytic active sites are the MoS_2 edges, and addition of a Ni promoter aids in increasing vacant sites by lowering the binding energy of sulfur present at the edges of MoS_2 (Byskov et al., 1997; Grimblot, 1998; Afanasiev and Bezverkhyy, 2007). To some extent, some research work has revealed that the final sulfided phase of the active catalyst is dependent on the extent to which the supported NiMo catalyst in its oxide form becomes sulfided since, sulfidation partially converts these oxide species into their equivalent active Ni (Co)-Mo-S structures. As a result, during catalyst formulation it is important to use a suitable metal composition that would optimize the metal loading on the support, and consequently result in the achievement of maximum hydrotreating activity (Prins et al., 1989; Furimsky, 1998; López and López, 2000).

The Ni (Co)-Mo-S structures exist in two forms (Type I and Type II). Usually, the Type II structure is more active than the Type I structure because, it is rarely attached to the support via Mo-O-Al linkages unlike, the Type I structure which is more bonded to the support. The linkages with the support create some steric hindrances during reactions and in the case of the Type II structure less linkage with the support results in less effect from steric hindrance which makes it easier for reactant molecules to access catalytic active sites. Comparatively, reactant molecules are more hindered from getting to the catalytic active sites in a Type I structure than a Type II structure. During hydrotreating an increase in temperature during sulfidation favors a Type II structure and hydrotreating activities since, stacking is enhanced as temperature increases and this further creates a highly active Type II structure (Vissers et al., 1987; Van Veen et al., 1993). Also, the presence of Type II structures can result in high activities because of their weak metal-support-interactions. Due to this, the use of carbon-supported catalyst in hydrotreating appears to be a good choice in terms of Type II structure formation because, the minimal support interaction that likely occurs makes it possible to sulfide these catalysts even under low temperature conditions into readily transformed Type II structures. On the other hand, for $NiMo/\gamma\text{-}Al_2O_3$ catalysts due to the strong metal support interaction sulfidation to Type II structures can be obtained using high sulfidation temperatures. Additionally, the properties at the active sites can be impacted by Mo loading since low Mo loadings are known to be dominated by Type I structures whereas, higher Mo loadings are dominated by Type II structures (Candia et al., 1984; Scheffer et al., 1986).

Use of carbon as a support in heterogenous catalysis has also attracted numerous attentions because of its relative chemical inertness, high porosity, high surface area, retention of its structural integrity, existence in various physical forms and ability to functionalize the carbon material to enhance catalytic activity. Many studies have also demonstrated that the use of carbon-supported catalysts leads to high HDS activities (Duchet et al., 1983; Rana et al., 2020). When given the choice to use carbon as a hydrotreating catalyst support, most researchers resort to carbon black or activated carbon because of their mass availability, low cost, and high surface area. In recent times a plethora of research related to the use of carbon in catalysis is centred around carbon nanotubes and fullerenes, and investigations about their properties and possible applications are still in progress. Use of carbon nanohorns (CNH) as a catalyst support is also in the limelight (Rodriquez-Reinoso, 1998; Falcao and Wudl, 2007; Titirici and Antonietti, 2010; Aryee et al., 2014; Lam and Luong, 2014; Aryee et al., 2021).

CNH is commonly produced using the arc-discharge method and is accompanied by the formation of a chunk by-product (termed OCP), and a fine fraction denoted as OCP_f in this study. For anodic type of arcs in which ablation of the anode is prevalent, these by-products usually form on the cathode and fall off or build up with time. Keidar et al. (2011) also added that for anodic arc, a carbonaceous deposit (~60–70% of the ablated material) inevitably forms on the cathode surface by reason of low thermal conductivity. This carbonaceous deposit can be described as having a crust-like texture with an inner black core that could contain carbon nanotubes, carbon nanoparticles and some graphitic particles. It is also noted to consist of a greyish metallic hard shell on the exterior with no nanotubes present. The appearance of this by-products after an arc experiment was also noted by Saito et al. (1993). In their work, they mentioned that a carbonaceous deposit made up of graphitic tubules and polyhedral particles accumulated on the face of the cathode electrode (Ebbesen and Ajayan, 1992; Saito et al., 1993; Tang et al., 2005; Keidar et al., 2011). Gattia et al. (2006) were of the view that the deposits collected on the cathode after conducting arc-discharge experiments comprised of CNH, CNT, amorphous carbon and carbon nanocages, and their results were not far-fetched from the observations from many arc discharge experiments that mentioned the formation of a rich multiwalled carbon nanotube (MWCNT) among the deposits on the surface of the cathode (Gattia et al., 2006; Arora and Sharma, 2014; Ng and Raitses, 2014; Yeh et al., 2016; Zhang et al., 2019). Yeh et al. (2016) also added that during the arc discharge process, the deposited carbonaceous material on the surface of the cathode and the walls of the reactor vessel contributed to the formation of nanoparticles by acting as an effective cathode electrode that sustained the arc discharge and reaction process. Results from their work also showed that a strong correlation exists between the radial distribution of the arc discharge current, temperature at the surface of the cathode deposit and the various morphologies of the deposits formed on the cathode. The complex nature of the formed nanoparticles is attributed to spatial variations of particle, plasma and heat fluxes from the arc to the deposit. The purity of the nanoparticles within the core area of the deposit are dependent on particle and heat flux from the plasma (Yeh et al., 2016).

The characteristics of the OCP produced in our laboratory and used in this phase of work matches the descriptions in the aforementioned paragraph. Our laboratory synthesis of CNH revealed that the OCP_f material can be simultaneously produced with CNH and the yield of OCP_f was more than twice the CNH material of interest. Also, from TEM analysis a micrograph of the OCP_f material showed that it comprises of CNH structures. Moreover, a feasibility study using OCP_f as a hydrotreating catalyst with Ni and Mo compositions of 2.5 wt % and 13 wt%, respectively resulted in an HDS activity of 78%

and an HDN activity of 25% (Aryee, 2019; Aryee et al., 2021). Thus, knowing the benefits of using carbon as a support, and having been convinced from other researchers that the by-products are mainly carbon-based particles. Our goals were to 1) enhance the hydrotreating performance of NiMo/OCP_f catalyst by experimenting different combinations of Ni and Mo that would lead to higher HDS and HDN activities and 2) to add value to an otherwise low-value by-product. To our knowledge, this low value by-product has not been attempted for utilization in the past. In addition, since the OCP_f material contains CNH materials, results from this hydrotreating study would help to determine the best bimetallic compositions to focus on in developing the best NiMo/CNH catalyst for hydrotreating.

MATERIALS AND METHODS

The average particle diameter of the OCP_f material used as the hydrotreating catalyst support in this study was 250 microns, and it was obtained after a particle separation step following a CNH arc discharge synthesis. In preparation for catalyst formulation, oxygenated functional groups were created on the OCP_f support by liquid oxidation. This step is important because it enhances the solubility of the support material and guarantees efficient wettability for metal anchorage since the catalyst preparation involved contacting the OCP_f material with catalyst precursor metals in solution. 30 min functionalization time emerged as the best duration for functionalizing OCP_f support material based on the results of a series of experimental runs to determine the best condition for OCP_f functionalization. Additionally, all OCP_f support material was functionalized for 30 min using the same method from a previous description (Aryee et al., 2014). The functionalized supports were then impregnated with Ni (2.5, 3.5 and 5.0 wt%) and Mo (13, 19 and 26 wt%) via the incipient wetness co-impregnation method from their respective aqueous metal precursor solutions containing requisite amount of nickel nitrate hexahydrate [$Ni(NO_3)_2{\cdot}6H_2O$], and ammonium heptamolybdate tetrahydrate [$(NH_4)6Mo_7O_{24}{\cdot}4H_2O$].

Seven (7) different OCP_f-supported catalysts were formulated for this study that were dependent on desired Ni and Mo loading combinations hence, for easy referencing the prepared catalysts were named as xNiyMo/OCP_f where; x is the wt% Ni composition and y is the wt% Mo composition used. The wet catalysts that were formulated were oven dried at 110°C overnight. Subsequently, each dried oxidic catalyst was ground and calcined in a furnace at 450°C for 5 h using argon as a carrier gas at 50 ml/min flow rate. Prior to hydrotreating experiments, 5 ml of each powdered catalyst was diluted with 12 ml of 90 mesh inert silicon carbide by way of loading into the reactor in 10–12 layers. Loading was done by alternating between catalyst and SiC and this method of loading in layers was utilized to ensure that both catalyst and inert material were distributed uniformly and can be reproduceable. Consequently, hydrodynamic conditions in the reactor are improved (Al-Dahhan et al., 1995; Mapiour et al., 2010). The top and bottom of the diluted catalyst mix was also packed with 3 mm glass beads, and different mesh sizes (16, 46 and 60) of silicon carbide. The packing was done in such a way that the diluent size increased as it approaches the top and bottom end of the reactor. After the reactor had been loaded, it was sealed firmly, and then transferred and mounted into the hydrotreater assembly. The hydrotreater was pressurized to ~9.3–9.7 MPa with helium and tested for leaks over 24 h.

In preparation for the hydrotreating experiments, the operating pressure was reduced to 9.0 MPa and kept constant throughout all experimental runs. The catalyst was wetted with a mixture of approximately 100 ml butanethiol (2.9 vol%) and insulating oil (500 ml). A sulfidation process continued for two consecutive days (48 h) after completion of catalyst wetting. Sulfidation temperatures of 193 and 343°C, respectively were used for each of the days, and an LHSV of 1 h^{-1} was maintained throughout the sulfidation process. Once sulfidation was complete, the sulfiding solution was switched to light gas oil and the catalyst was precoked for 3 days at an LHSV of 2 h^{-1} and a temperature of 370°C. Thereafter, the hydrotreating tests were executed at three different temperatures (i.e., 330, 350 and 370°C). Each experimental temperature condition was run for 1.5 days and a constant LHSV and pressure of 2 h^{-1} and 9.0 MPa, respectively were maintained for all the runs. Hydrotreated liquid samples were collected after every 12 h. However, a change in experimental temperature condition led to the discarding of collected samples for the initial 12 h of run before any further storage was done. The collected samples were stripped for 2 h with N_2 gas to eliminate the presence of any residual traces of NH_3 and H_2S in the liquid sample. Sulfur and nitrogen concentrations in the stripped liquid products were further analyzed with the Antek 9000 NS analyzer.

CHARACTERIZATION

N_2 Adsorption-Desorption Isotherms

The porous structure of all calcined catalysts was determined using the BET-Micromeritics ASAP 2020 surface area and porosity analyzer. Both the adsorption and desorption isotherm branches, and nitrogen gas adsorbed at 77 K were taken into consideration in the analysis. The Brunauer-Emmett-Teller (BET) method was used in calculating the surface areas whereas, the total pore volume and pore size distribution were determined by the Barett-Joyner-Halenda (BJH) method. Approximately 0.1 g of each sample was outgassed at 200 °C to a residual pressure of $<6.6 \times 10^{-4}$ Pa prior to adsorption.

Thermogravimetric Analysis (TGA)

Thermal stabilities of catalyst samples that had been dried and calcined were analyzed using a TA Q500 series instrument with simultaneous thermogravimetric analysis (TGA)/differential scanning calorimeter (DSC) application. The analysis was carried out by heat treating approximately 15 mg of sample

from room temperature to 700 °C at 10°C/min ramp rate and the flow rate of nitrogen used was 60 ml/min.

X-Ray Diffraction (XRD) Analysis

The structure, crystallinity and phase of catalyst samples were examined by XRD analysis with the Bruker D8 Advance powder X-ray diffractometer using CuKα radiation (λ = 0.1541 nm). The X-ray gun was powered at 30 mA and 40 kv. Bragg angle (2θ) was scanned from 1.5 to 10° for low angle X-ray diffraction, and from 10 to 80° for wide angle X-ray diffraction. The sample weight for analysis was about 0.25 g.

CO-Chemisorption

An ASAP 2020 micrometrics instrument was used in conducting CO chemisorption analysis and this enabled the percentage metal dispersion to be calculated in relation to carbon monoxide uptake measured on each catalyst. About 0.10 g of each catalyst sample which had previously undergone a degassing step for 60 min at 110°C was further reduced *in situ* under hydrogen flow for 2 h at 350°C. Thereafter, the reduced sample was cooled to 35°C and consequently evacuated after attaining a static pressure of less than 1.3×10^{-5} Pa. CO chemisorption measurements corresponding to CO uptake at 35°C were done after CO pulses had passed over the sample. For bimetallic catalysts, **Eq. (1)** was used in calculating the percentage metal dispersion of the active metals that are available and interact with the adsorbate.

$$\%M_{DISP} = \frac{1}{22414^*} \times \frac{V \text{ x } SF_{CALC}}{\frac{wt.fraction\,M_O}{W_{ATOMIC,M_O}} + \frac{wt.\ fraction\,N_i}{W_{ATOMIC,N_i}}} \quad (1)$$

where, $\%M_{DISP}$ = percentage metal dispersion, SF_{CALC} = calculated stoichiometry factor, $W_{ATOMIC,\ Mo}$ = atomic weight of first metal, Mo (g/mole), $W_{ATOMIC,\ Ni}$ = atomic weight of second metal, Ni (g/mole), V = volume intercept that was obtained from the line of best fit to the differences in volume between the selected points of the first analysis and the repeated analysis (cm^3/g STP), *The volume occupied by 1 mol of gas (cm^3 STP/mole of gas) (Micromeritics ASAP, 2020).

High Resolution Transmission Electron Microscopy (HRTEM)

The morphology of each catalyst was analyzed using a JEOL 2011 (200 kv) scanning transmission electron microscope (STEM). In preparation for the analysis, catalyst samples were ground to fine particle size and then a minute quantity was dispersed onto a 200-mesh holey carbon-coated TEM support grid. For every sample, about 5–10 representative images were taken at low to high magnification ranging from 20–250 k times magnification.

Temperature Programmed Reduction (TPR)

H_2-temperature programmed reduction (H_2–TPR) analysis was conducted in a TPD/TPR Quantachrome AutosorbiQ (United States) equipment to evaluate how the reducibility of the metal species in the catalyst behaved. The gas mixture used in conducting the analysis comprised of 3% H_2/N_2 (v/v). A catalyst sample weight of 0.1 g was used for the analysis. The TPR analysis procedure involved these steps i.e., purging the sample with helium (He) at 400 °C for an hour to pre-treat the sample, cooling to room temperature, followed by ramping the program from room temperature to 800°C at a ramp rate of 10°C/min as the reducing gas mixture flowed at 30 ml/min. A thermal conductivity detector enabled the monitoring of the hydrogen consumption within the temperature range of interest.

Sulfur and Nitrogen Removal

Total S and N compositions for both untreated and treated gas oil samples were determined using the Antek 9000 NS analyzer. A combustion/fluorescence technique together with the ASTM D5463 standard procedure was used in analyzing the sulfur removal whereas, a combustion/chemiluminescence technique and the ASTM D4629 standard procedure was used to analyze the nitrogen removal.

RESULTS AND DISCUSSION

BET Analysis of Pristine OCP_f, Functionalized OCP_f and OCP_f-Supported NiMo Catalysts

Table 1 shows the surface area, pore volume and pore diameter of as-synthesized OCP_f, functionalized OCP_f, and NiMo/OCP_f catalysts with varying Ni and Mo compositions. The functionalized OCP_f material was found to be of higher surface area and pore volume than the pristine OCP_f due to the presence of defects after functionalization. Contrarily, a decrease in pore diameter was rather observed as the pristine OCP_f material was functionalized, and this was due to the breaking of bigger pores, with the average pore diameter being more representative of smaller pores (Karousis et al., 2016). For the different catalysts it was observed that the surface area and pore volume of all the catalysts decreased from the functionalized material due to the plugging of pores by metals. An increment in pore diameter however, occurred after the functionalized OCP_f samples had been impregnated with metals to form different catalysts.

There was no significant change in surface area at constant Ni composition of 2.5 wt% as Mo composition was raised from 13 wt % to 19 wt%. On the other hand, as the Ni loading was kept constant at higher compositions (either 3.5 wt% or 5.0 wt%), increased in Mo composition from 13 wt% to 19 wt% resulted in ~16% decrease in surface area. This is because more pores were blocked as higher Mo loadings were impregnated on the support. Keeping the Mo loading constant at a lower composition of 13 wt % did not bring about any significant change in surface area and pore diameter at increasing Ni composition from 2.5 wt% to 3.5 wt%. However, at a constant Mo loading of 19 wt% both the surface area and pore diameter decreased steadily as Ni compositions increased from 2.5 to 3.5 wt%. Also, the decrease in surface area was significant under this condition. Overall, almost all the catalysts exhibited mesoporous pore diameters and constant pore volume. Unlike all other catalysts, the 5.0wt% Ni26wt%Mo/OCP_f catalyst with the highest Ni and Mo

TABLE 1 | BET analysis of pristine OCP_f, functionalized OCP_f, and NiMo/OCP_f catalysts.

Sample	BET surface area (m^2/g)	Pore volume (cm^3/g)	Pore diameter (nm)
Pristine OCP_f	41 ± 2	0.15 ± 0.01	22.1 ± 0.2
Functionalized OCP_f	177 ± 2	0.19 ± 0.01	9.3 ± 0.1
2.5wt%Ni13wt%Mo/OCP_f	97 ± 1	0.12 ± 0.01	10.1 ± 0.2
2.5wt%Ni19wt%Mo/OCP_f	99 ± 2	0.14 ± 0.01	12.8 ± 0.1
3.5wt%Ni13wt%Mo/OCP_f	96 ± 2	0.12 ± 0.01	9.6 ± 0.1
3.5wt%Ni19wt%Mo/OCP_f	81 ± 2	0.12 ± 0.01	11.1 ± 0.1
5.0wt%Ni13wt%Mo/OCP_f	106 ± 2	0.12 ± 0.01	10.6 ± 0.1
5.0wt%Ni19wt%Mo/OCP_f	89 ± 2	0.12 ± 0.01	10.9 ± 0.1
5.0wt%Ni26wt%Mo/OCP_f	78 ± 2	0.12 ± 0.01	12.6 ± 0.2

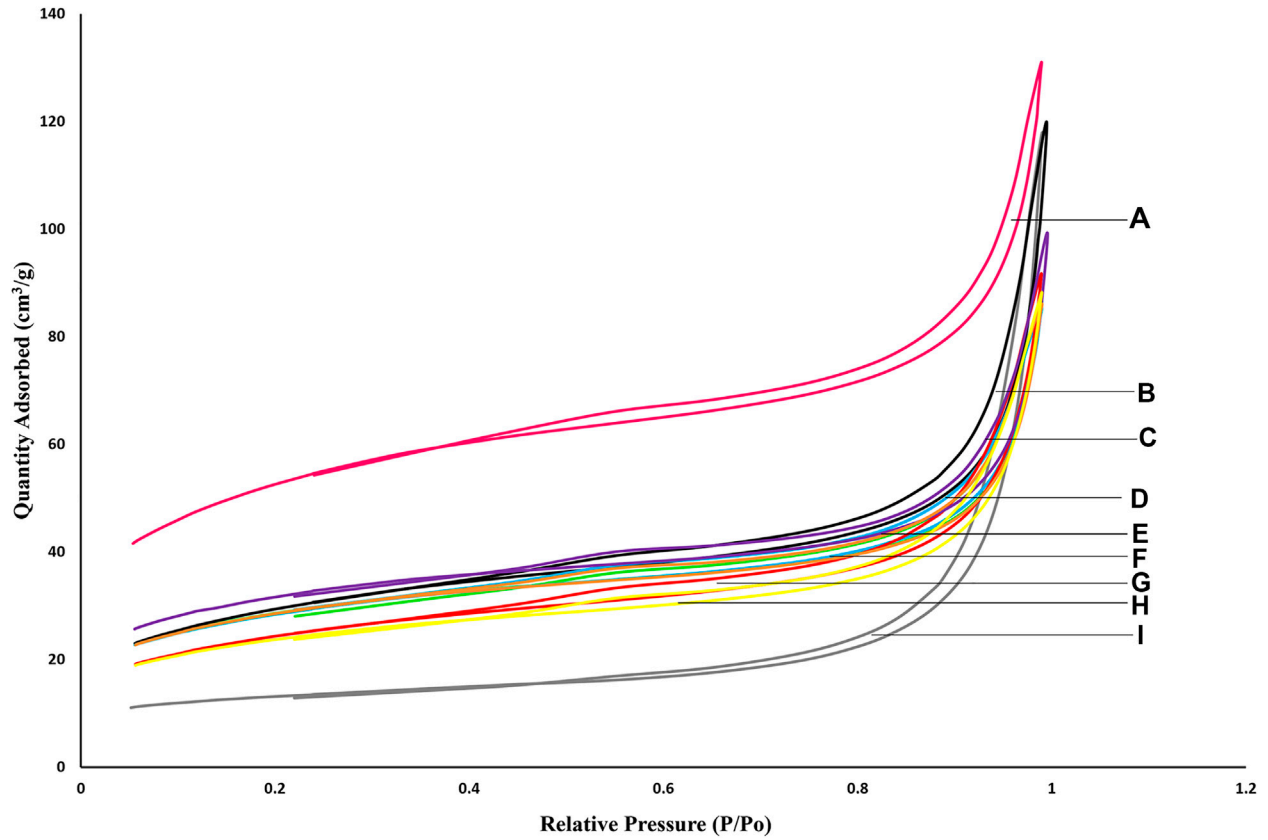

FIGURE 1 | Adsorption-desorption isotherms of OCP_f-supported NiMo catalysts **(A)** Functionalized OCP_f **(B)** 2.5wt%Ni19wt%Mo/OCP_f **(C)** 5.0wt%Ni13wt%Mo/OCP_f **(D)** 2.5wt%Ni13wt%Mo/OCP_f **(E)** 5.0wt%Ni19wt%Mo/OCP_f **(F)** 3.5wt%Ni13wt%Mo/OCP_f **(G)** 3.5wt%Ni19wt%Mo/OCP_f **(H)** 5.0wt%Ni26wt%Mo/OCP_f, **(I)** Pristine OCP_f.

compositions exhibited the lowest surface area since its pores were filled with metals having the highest weight compositions during catalyst formulation. Consequently, its pore diameter was high since it was more likely for its micropores to be blocked making its mesopores the major representative of its pore diameter.

The adsorption-desorption isotherms of pristine OCP_f, functionalized OCP_f and all the NiMo/OCP_f catalysts used in this study are shown in **Figure 1**.

From **Figure 1** all the samples tested displayed Type IV isotherm which is typical of mesoporous materials but with H3 hysteresis loop. Among all the samples, the functionalized OCP_f exhibited higher adsorption capabilities because of the nanowindows created on the support material as well as the consequent increase in surface area after acid treatment. The pristine OCP_f sample showed minimal adsorption capabilities compared to the rest of the samples. From **Figure 1**, the shapes of the functionalized adsorption-desorption isotherm and that of

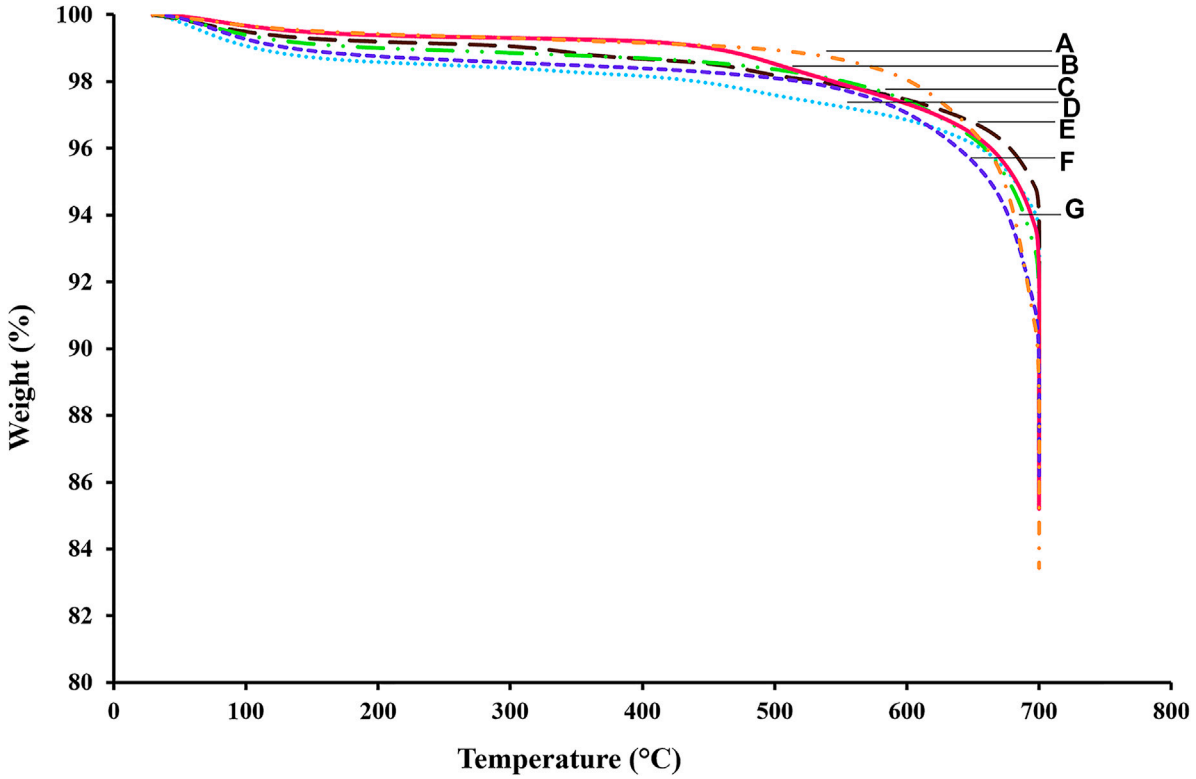

FIGURE 2 | TGA profiles of OCP$_f$-supported NiMo catalysts **(A)** 5.0wt%Ni19wt%Mo/OCP$_f$ **(B)** 3.5wt%Ni19wt%Mo/OCP$_f$ **(C)** 3.5wt%Ni13wt%Mo/OCP$_f$ **(D)** 2.5wt %Ni13wt%Mo/OCP$_f$ **(E)** 2.5wt%Ni19wt%Mo/OCP$_f$ **(F)** 5.0wt%Ni13wt%Mo/OCP$_f$ **(G)** 5.0wt%Ni26wt%Mo/OCP$_f$.

the various catalysts were similar and this implies that the pore structure of the functionalized OCP$_f$ material remained intact in all the catalysts (Sing et al., 1985). The highly loaded catalysts are practically a mixture of well dispersed catalysts and some remnants of crystalline NiMo phase.

TGA Analysis of the OCP$_f$-Supported NiMo Catalysts

Since all OCP$_f$ catalysts were prepared from a by-product support and there is an instant negativity surrounding by-products, the thermal stability of the catalysts had to be tested with TGA at the hydrotreating temperature conditions (330, 350 and 370°C) being experimented to ensure that the catalysts would not burn out during the hydrotreating process. Thus, **Figure 2** displays the TGA profiles of all the calcined OCP$_f$-supported NiMo catalysts utilized in this study.

Removal of nitrates, ammonia and water in an impregnated catalyst sample is prevalent during TGA analysis, and nitrates present in carbon-supported catalysts could cause oxidation of carbon support. It is also worth noting that with respect to calcination, carbon supports are prone to oxidation as NH_3 is removed during a calcination step which is catalyzed by Mo deposits. Thus, oxidation of carbon supports can be prevented by low temperature calcination of the catalyst in air or by calcination in an inert environment. Another way to prevent oxidation of the catalyst is to use a presulfided catalyst that does not decompose $(NH4)_6Mo_7O_{24}$. Additionally, oxidation of carbon supports can be prevented by impregnation of the support with a MoO_3/water slurry in place of $(NH4)_6Mo_7O_{24}$/water solution. For the MoO_3/water slurry or slurry, impregnation method calcination is not required because although the solubility of MoO_3 is low, molybdena species are gradually transported and adsorbed onto the carbon surface because of electrostatic attraction between molybdate anions and positively charged carbon surfaces (Vissers et al., 1987; Kaluža, and Zdražil, 2001). Work by Vissers et al., 1987 confirmed that direct sulfidation of an uncalcined carbon-supported catalyst with a sulfiding agent preferably H_2S/H_2 mixture impedes carbon destruction due to the lack of gasification of the carbon support to methane or CO (Vissers et al., 1987).

From **Figure 2** the desorption of water that had been physically adsorbed led to a weight loss of about 1% up to 120°C. Afterwards, the weight loss was almost constant up to about 400°C and mostly stable until ~600°C. The stability of the thermal properties from 120–400°C may be due to less concentration of surface defects on the catalysts. A slight loss in weight from 120–400°C can be attributed to the loss of impurities that remain on the sample after catalyst preparation, or loss due to MoO_3 decomposition into MoO_2 or $Mo4O_{11}$ intermediate compounds (Spevack and

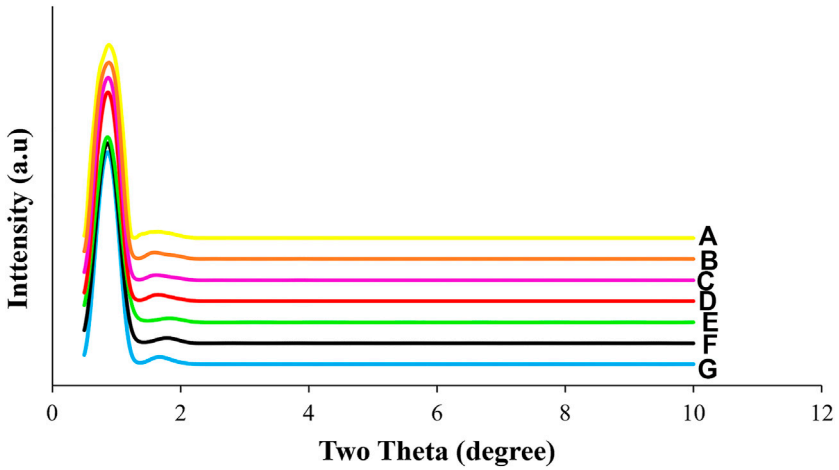

FIGURE 3 | Low angle XRD patterns of OCP$_f$-supported NiMo catalysts **(A)** 5.0wt%Ni26wt%Mo/OCP$_f$ **(B)** 5.0wt%Ni19wt%Mo/OCP$_f$ **(C)** 5.0wt%Ni13wt%Mo/OCP$_f$ **(D)** 3.5wt%Ni19wt%Mo/OCP$_f$ **(E)** 3.5wt%Ni13wt%Mo/OCP$_f$ **(F)** 2.5wt%Ni19wt%Mo/OCP$_f$ **(G)** 2.5wt%Ni13wt%Mo/OCP$_f$.

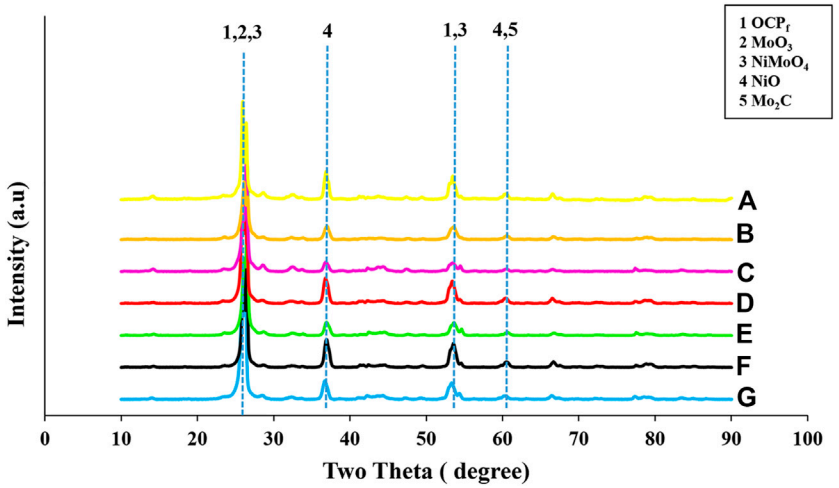

FIGURE 4 | High angle XRD patterns of OCP$_f$-supported NiMo catalysts **(A)** 5.0wt%Ni26wt%Mo/OCP$_f$ **(B)** 5.0wt%Ni19wt%Mo/OCP$_f$ **(C)** 5.0wt%Ni13wt%Mo/OCP$_f$ **(D)** 3.5wt%Ni19wt%Mo/OCP$_f$ **(E)** 3.5wt%Ni13wt%Mo/OCP$_f$ **(F)** 2.5wt%Ni19wt%Mo/OCP$_f$ **(G)** 2.5wt%Ni13wt%Mo/OCP$_f$.

Mcintyre, 1992; Serp et al., 2003). Beyond 500°C–700°C carbothermal reductive decomposition of NiO or $NiMoO_4$ may contribute to the weight loss (Lebukhova and Karpovich, 2008). The drastic drop in weight for all the NiMo/OCP$_f$ catalyst samples at about 700°C can also be attributed to the findings from Bekyarova et al. (2002) which showed that at higher temperatures of at least 500°C, carbon nanomaterials are prone to burn-off due to instability. Although, an inert gas (nitrogen) was used to carry out the TGA experiments the thermal stability of the catalyst in terms of thermal sintering is the same regardless of the reactive gas environment (H_2) used during hydrotreating since, exposure to higher (>500°C) gas-phase temperatures is the main factor that influences catalyst deactivation by thermal sintering (Bartholomew, 2001; Bekyarova et al., 2002; Fogler, 2006). Based on the above information the thermal stability of all the catalysts in terms of thermal sintering is assured for the hydrotreating temperatures (330–370°C) being studied.

XRD Analysis of the OCP$_f$-Supported NiMo Catalysts

Low angle XRD profile patterns of all the different NiMo/OCP$_f$ catalysts displayed in **Figure 3** shows a hexagonal mesoporous

TABLE 2 | CO-chemisorption analysis of all the OCP_f-supported NiMo catalysts.

Catalysts	Metal dispersion (%)	CO absorbed (μmol/g)	Crystallite size (nm)
2.5wt%Ni13wt%Mo/OCP_f	5.8 ± 0.2	102 ± 2	21.6 ± 0.2
2.5wt%Ni19wt%Mo/OCP_f	4.4 ± 0.2	106 ± 1	28.5 ± 0.2
3.5wt%Ni13wt%Mo/OCP_f	6.2 ± 0.2	121 ± 2	19.7 ± 0.2
3.5wt%Ni19wt%Mo/OCP_f	6.2 ± 0.2	158 ± 2	20.1 ± 0.2
5.0wt%Ni13wt%Mo/OCP_f	9.3 ± 0.2	205 ± 2	12.9 ± 0.2
5.0wt%Ni19wt%Mo/OCP_f	7.8 ± 0.1	221 ± 2	15.7 ± 0.2
5.0wt%Ni26wt%Mo/OCP_f	3.8 ± 0.2	135 ± 1	32.6 ± 0.3

structure with well resolved strong (2θ = 0.9) and weak (2θ = 1.7) peaks that were identical for every catalyst used in this study. The peaks were indexed at d (100) and d (110). This identical characteristic implied that variation in metal loading composition did not influence the hexagonal mesoporous structure.

Figure 4 shows the high angle XRD profile patterns of all the NiMo/OCP_f catalysts, and the XRD diffractograms revealed crystalline phases for all samples. The 2θ diffraction peak at ~ 26° represents, (002) plane characteristic of a hexagonal carbon structure. This 2θ diffraction peak at ~26° also corresponds to an intense MoO_3 and $NiMoO_4$ peak. Thus, the peak at this position can be associated to an overlap of carbon (OCP_f), MoO_3 and $NiMoO_4$ material. Other small intensity peaks occurred at ~37° and ~54° on all the catalysts which corresponded to NiO and $NiMoO_4$, respectively. The appearance of these characteristic crystalline peaks relating to MoO_3, NiO and $NiMoO_4$ on the OCP_f-supported NiMo catalysts implied that the metals were not well dispersed on the support. A small diffraction peak relating to molybdenum carbide (Mo_2C) was also observed at 2θ = ~61° (Quanli et al., 2003; Gattia et al., 2006; Liu et al., 2011; Aryee et al., 2021). The crystal sizes of all the catalysts were calculated from all XRD patterns using the Derbye-Scherrer equation. These values ranged from 8 to 14 nm. For the 5.0wt%Ni19wt%Mo/OCP_f catalyst, the crystal sizes were calculated using peaks at two theta values of 26°, 37°, 54° and 61° in **Figure 4**. Also, the crystal sizes of the NiO phase for 2.5wt%Ni13wt%Mo/OCP_f, 2.5wt%Ni19wt%Mo/OCP_f, 3.5wt%Ni13wt%Mo/OCP_f, 3.5wt%Ni19wt%Mo/OCP_f, 5.0wt%Ni13wt%Mo/OCP_f, 5.0wt%Ni19wt%Mo/OCP_f and 5.0wt%Ni26wt%Mo/OCP_f catalysts were calculated, which varied from 11–13 nm.

The crystalline peak intensities exhibited by the 5.0wt%Ni13wt%Mo/OCP_f, 5.0wt%Ni19wt%Mo/OCP_f, 3.5wt%Ni13wt%Mo/OCP_f and 2.5wt%Ni13wt%Mo/OCP_f catalysts were smaller than the rest of the catalysts hence, it is expected that the dispersion of the metal components in these catalysts would be much improved compared to the remaining OCP_f-supported NiMo catalysts used in this study. Additionally, this result implies that an improved dispersion can be obtained if a catalyst is formulated using a combination of Ni compositions varying from 2.5 to 5.0 wt% and a low Mo composition of 13 wt%. However, for a high Mo composition of 19 wt% an improved dispersion can also be achieved with a high Ni composition of 5.0 wt%.

CO-Chemisorption Analysis of the OCP_f-Supported NiMo Catalysts

Results from CO-chemisorption analysis are displayed in **Table 2**, and these results show that at constant Ni composition of 2.5 and 5.0 wt%, an increase in Mo composition from 13 wt% to 19 wt% resulted in a decrease in dispersion and a corresponding increase in CO uptake. Nonetheless, no change in dispersion occurred at constant Ni composition of 3.5 wt% as the Mo varied from 13 to 19 wt%. However, at constant Mo loadings of 13 wt% or 19 wt%, metal dispersion and CO uptake increased steadily with increasing Ni compositions from 2.5 to 5.0 wt%. This positive impact is ascribed to the fact that increase in Ni loadings increases the amount of Ni release during sulfidation, and this effect simultaneously enhances the redistribution of MoO_3 which further results in a decrease in crystallite size with a corresponding increase in metal dispersion (Badoga et al., 2014). Results from **Table 2** also indicate that of all the catalyst under study a significant improvement in both metal dispersion and CO uptake can be achieved by using a catalyst with high Ni composition (5.0 wt%) and an Mo composition of either 13 wt% or 19 wt%. Thus, the 5.0wt%Ni13wt%Mo/OCP_f and 5.0wt%Ni19wt%Mo/OCP_f catalysts exhibited maximum metal dispersions whereas, the 5.0wt%Ni26wt%Mo/OCP_f catalyst showed the least metal dispersion since, the Mo loadings of 26 wt% was too high for the 5.0 wt% Ni to have any positive influence on the redistribution of MoO_3 to form smaller crystallite size with enhanced dispersion.

The average diameter (nm) of the crystallites (assumption-spherical) is given by this equation $d = \frac{6.10^3}{\rho M}$ where, M = metallic surface area (m^2/g), ρ = the specific mass of the metal (g/cm^3), (Lynch, 2003).

HRTEM Examination of the Morphology of the Various OCP_f-Supported NiMo Catalysts

The morphology of the different NiMo/OCP_f catalysts used for this study are displayed in **Figure 5**. The TEM micrographs of all the catalysts showed dark spots that signified that indeed metals have been impregnated on the support. However, the micrographs suggest that metals were not evenly dispersed on the support. Additionally, apart from CNH structures, some of the catalysts also revealed CNT and other embedded structures typical of an OCP_f material (Gattia et al., 2006; Zhang et al., 2019).

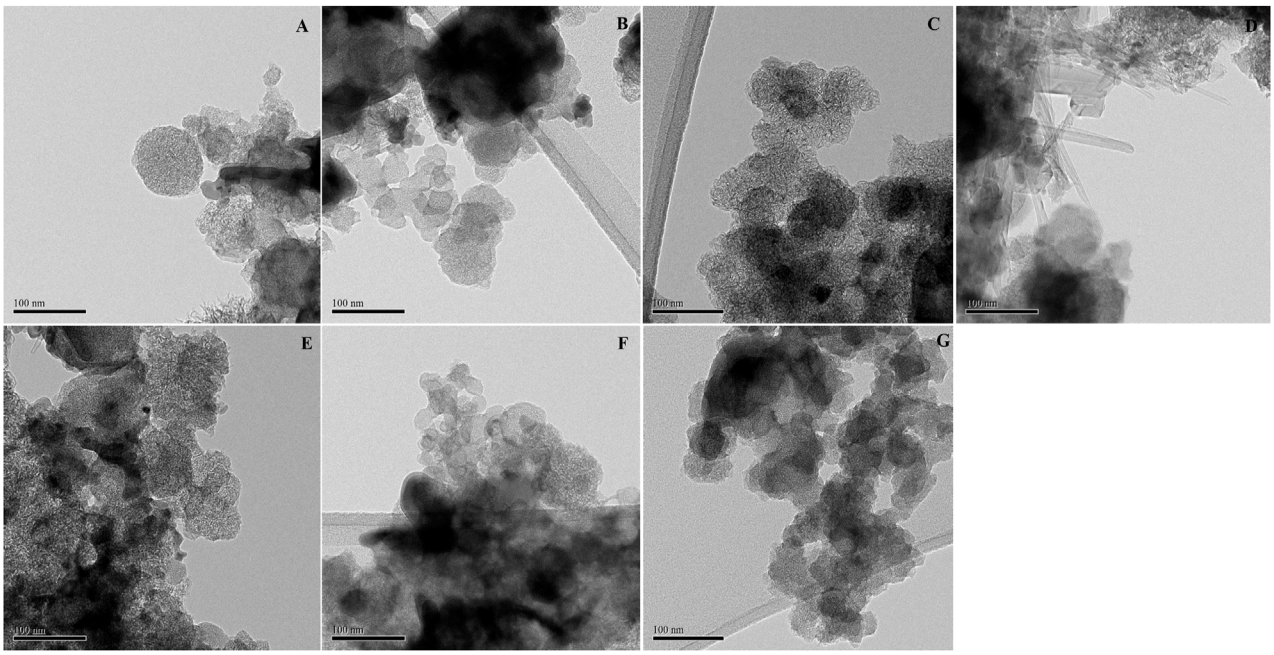

FIGURE 5 | Morphology of different NiMo/OCP$_f$ catalysts **(A)** 2.5wt%Ni13wt%Mo/OCP$_f$ **(B)** 2.5wt%Ni19wt%Mo/OCP$_f$ **(C)** 3.5wt%Ni13wt%Mo/OCP$_f$ **(D)** 3.5wt%Ni19wt%Mo/OCP$_f$ **(E)** 5.0wt%Ni13wt%Mo/OCP$_f$ **(F)** 5.0wt%Ni19wt%Mo/OCP$_f$ **(G)** 5.0wt%Ni26wt%Mo/OCP$_f$.

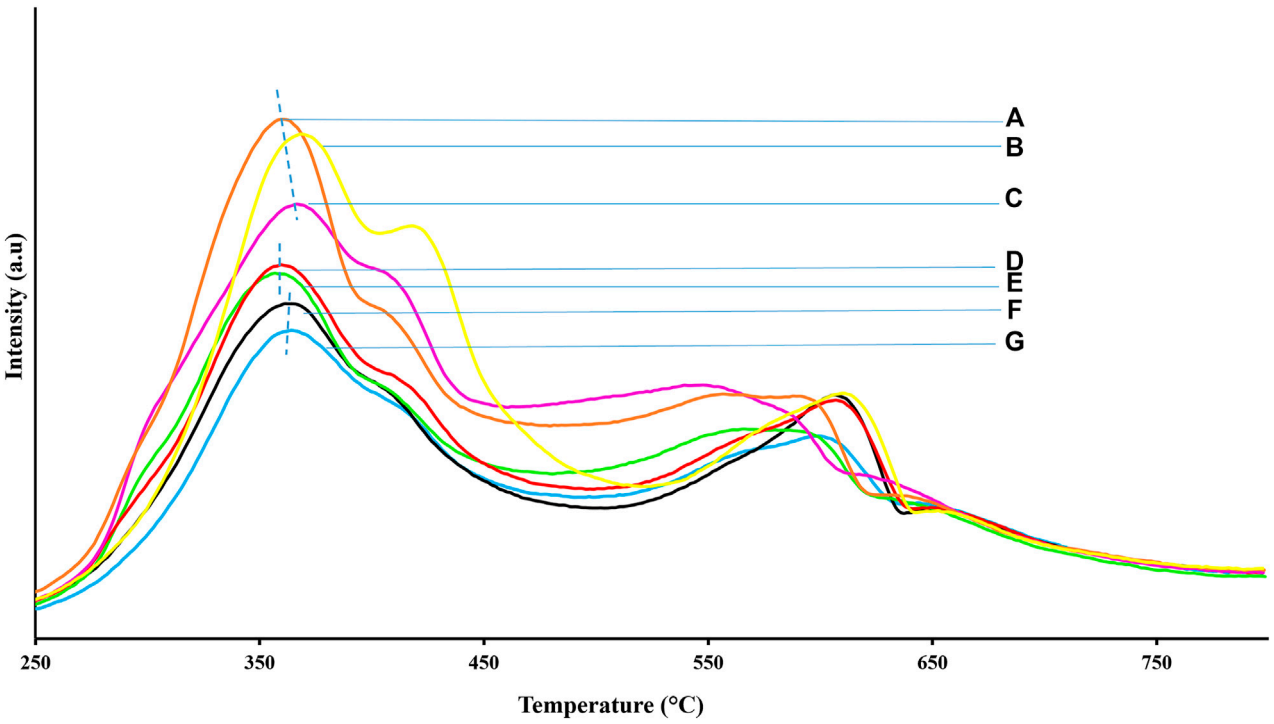

FIGURE 6 | TPR results of NiMo/OCP$_f$ catalysts; **(A)** 5.0wt%Ni19wt%Mo/OCP$_f$, **(B)** 5.0wt%Ni26wt%Mo/OCP$_f$, **(C)** 5.0wt%Ni13wt%Mo/OCP$_f$, **(D)** 3.5wt%Ni19wt%Mo/OCP$_f$, **(E)** 3.5wt%Ni13wt%Mo/OCP$_f$, **(F)** 2.5wt%Ni19wt%Mo/OCP$_f$, **(G)** 2.5wt%Ni13wt%Mo/OCP$_f$.

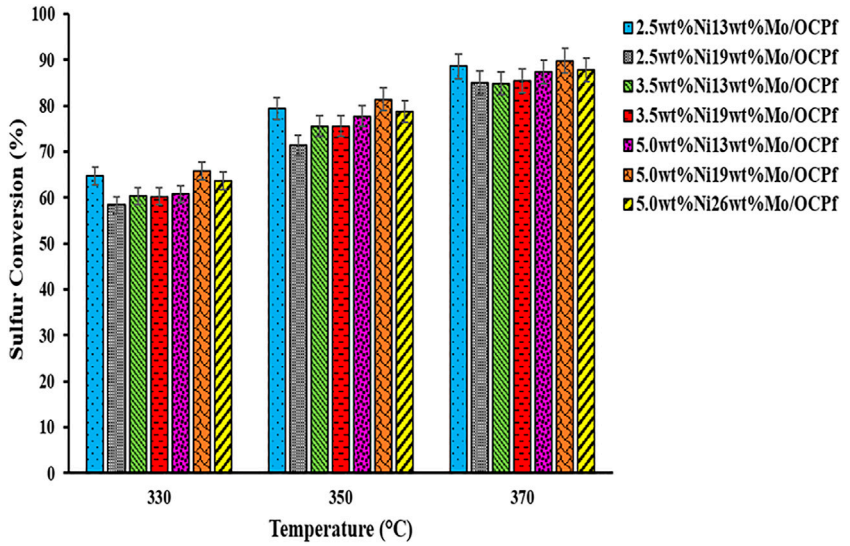

FIGURE 7 | HDS activities of NiMo/OCP$_f$ catalysts with LGO at 330, 350, and 370°C (Catalyst = 5 cm^3, LHSV = 2 h^{-1}, P = 9.0 MPa, and H_2/oil ratio = 600 (ml/ml)).

TPR Analysis of the Various OCP$_f$-Supported NiMo Catalysts

The TPR results of all the NiMo/OCP$_f$ catalysts are shown in **Figure 6**. Two Mo reduction peaks at low (320–394°C) and high (570–660°C) temperature values were detected. The first peak corresponded to a partial reduction of Mo^{6+} to Mo^{4+} whereas the second peak was from a combination of a complete reduction of Mo^{6+} to Mo^{4+} and Mo^{4+} to Mo^{0+}. Reduction of Ni^{2+} also contributed to the low temperature reduction peak in the range of 250–375°C whereas, $NiMoO_4$ also contributed to the reduction peak that ranged from 375 to 480°C (Hurst et al., 1982; Brito et al., 1989; Calafat et al., 1996; Aryee et al., 2021). All the catalysts revealed the presence of crystalline MoO_3 in the shoulder of the first peak and on the high temperature side. This is a typical position for crystalline MoO_3 and normally the absence of this peak signifies that MoO_3 is amorphous and/or well dispersed. As a result, it is obvious that the most overloaded catalyst is 5.0wt%Ni26wt%Mo/OCP$_f$ due to the high intensity of the MoO_3 crystalline peak and the shift of this peak towards a higher temperature. The preceding information correlates well with the XRD patterns, CO chemisorption dispersion results as well as the overall activity results from all catalysts (Regalbuto and Ha, 1994; Qu et al., 2003).

Overall, except for the 5.0wt%Ni26wt%Mo/OCP$_f$ catalyst that revealed a first peak reduction temperature at 372°C, the first peak reduction temperature for all the remaining catalysts under study was centered around 362°C. Thus, the 5.0wt%Ni26wt%Mo/OCP$_f$ catalyst with the highest Ni and Mo composition among all the catalysts under study exhibited the greatest difficulty in reduction. Also, for the remaining catalysts it can be inferred that variation of Ni and Mo in any of these catalyst combinations only resulted in a slight change in the first peak reduction temperature and consequently the effect of metal support interaction from these catalysts may have similar impact on hydrotreating performance. However, the hydrogen consumption intensity increased drastically as Ni compositions increased from 2.5 to 5.0 wt% as compared to the slight jump in hydrogen consumption intensity with increasing Ni composition from 2.5 to 3.5 wt%. From **Figure 6**, it was obvious that hydrogen consumption intensities were also higher for the catalysts with 19 wt% Mo compositions than catalysts with Mo compositions of 13 wt% since more active sites were present in the former than the later. (Grimblot, 1998; Afanasiev and Bezverkhyy, 2007). Additionally, the high MoS_2 active sites accompanying high compositions aided in shifting the peaks to lower temperatures as in the case of the 5.0wt%Ni13wt%Mo/OCP$_f$ and 5.0wt%Ni19wt%Mo/OCP$_f$ catalysts.

The catalysts with 5.0 wt% Ni composition are expected to have high HDS and HDN activities because, the highest hydrogen consumption intensities displayed by these catalysts especially in the case 5.0wt%Ni19wt%Mo/OCP$_f$ catalyst is advantageous since this characteristic renders the MoO_3 present in these catalysts, to undergo rapid transformation to a Type II Ni-Mo-S phase associated with enhanced activity (Park et al., 1997; Yin et al., 2011). This assertion from TPR analysis implies that the hydrogen consumption intensities, which indicate higher extent of reducibility of MoO_3 species, can have a significant impact on creating Type II Ni-Mo-S phase and inducing higher hydrotreating performance. From the TPR study, it is also noted that the metal-support-interaction is slightly impacted by variation in metal loadings on OCP$_f$-supported catalysts due to similarities in the first peak reduction temperature values displayed by these catalysts in **Figure 6**.

HDS and HDN Activities of the Various OCP$_f$-Supported NiMo Catalysts

Figure 7 and **8** show the results of the effects of temperature on the HDS and HDN activities of all the different catalysts after a

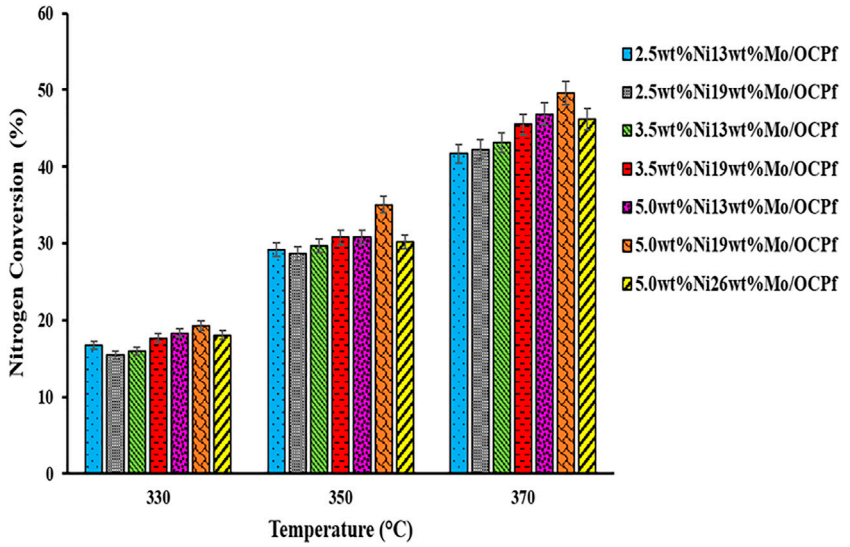

FIGURE 8 | HDN activities of NiMo/OCP$_f$ catalysts with LGO at 330, 350, and 370°C (Catalyst = 5 cm^3, LHSV = 2 h^{-1}, *P* = 9.0 MPa, and H_2/oil ratio = 600 (ml/ml)).

rigorous long-lasting test. Overall, although small differences in activity results were realized the results are very meaningful. In all cases, both HDS and HDN activities increased with increasing temperature. A rise in HDS and HDN activities with increasing temperature is attributed to higher reaction rates and conversions accompanying an increase in temperature (Speight, 2000). Thus, maximum HDS and HDN activities were obtained at the highest operating temperature of 370°C. Overall, the activity results of all catalysts revealed that HDS processes exhibited higher activities than the HDN processes under the different temperature conditions. This trend is acceptable because, it is much easier to convert sulfur compounds with less refractory linkages than total nitrogen compounds comprising of the most refractory compounds. Total nitrogen compounds in gas oils exist in two forms i.e. basic and non-basic nitrogen compounds, and in terms of activity the non-basic nitrogen compounds contribute to the low activities exhibited by total nitrogen compounds since they are less reactive (Laredo et al., 2001; Botchwey et al., 2003; Sano et al., 2004).

Results from **Figure 7** shows that at 370°C, the HDS activities for the 2.5wt%Ni19wt%Mo/OCP$_f$, 3.5wt%Ni13wt%Mo/OCP$_f$, and 3.5wt%Ni19wt%Mo/OCP$_f$ catalysts were almost the same (~85%). However, these catalysts exhibited a steady increase in HDN activities as depicted in **Figure 8**. Also, from **Figure 7** doubling the compositions of Ni and Mo as in the case of the 2.5wt%Ni13wt%Mo/OCP$_f$ catalyst and 5.0wt%Ni26wt%Mo/OCP$_f$ catalyst did not double the conversions in a direct scale up manner. Activity results from these two catalysts indicated that a slight decrease (~1%) in HDS activities occurred when the Ni and Mo compositions were doubled, whereas a slight increase (~4%) in HDN activities occurred by doubling the metal compositions. This implies that doubling the metal compositions have insignificant impact on the conversions as it overloads the support with crystalline phase, therefore not a good choice in catalyst formulation.

For the 2.5wt%Ni13wt%Mo/OCP$_f$ catalyst, although the use of this catalyst in the preliminary study mentioned in the abstract and reported elsewhere resulted in an HDS and HDN activity of 78 and 25%, respectively the HDS and HDN activities further increased to 89 and 42% using the same catalyst composition and light gas oil in this study. The enhancement of the catalyst activities in this study can be attributed to an improvement in textural properties, percentage dispersion and reducibility brought about by a reduction in particle size after sieving since, more fine materials with better characteristics were collected and used for catalyst formulation by using a particle cut-off size of 250 microns in this study versus a particle cut-off size of 297 microns used in the preliminary study. Additionally, the improvement in HDS and HDN activities for the 2.5wt% Ni13wt%Mo/OCP$_f$ catalyst used in this study may be due to the LHSV value 1 h^{-1}, which was used in sulfiding the catalyst in this study prior to all hydrotreating experiments compared to LHSV value of 2 h^{-1} used in sulfiding a similar catalyst composition in the preliminary study (Aryee et al., 2021). Less LHSV means more contact time between the catalyst and liquid during sulfidation, and this increases the active sites with subsequent increase in activities (Satterfield, 1991). Findings from this work also demonstrated that high HDS activities can be achieved with a NiMo/OCP$_f$ catalyst having lower metals loading (2.5 wt% Ni and 13 wt% Mo) and/or higher metals loading (5.0 wt% Ni and 19 wt% Mo).

On the other hand, it was found that among all the catalyst used in this study use of the 5.0wt%Ni19wt%Mo/OCP$_f$ catalyst led to the highest hydrotreating performance for both HDS (90%) and HDN (50%) activities due to its high ability to consume hydrogen (TPR results) that translates to easier formation to a Type II Ni-Mo-S phase with enhanced activity (Yin et al., 2011; Park et al., 1997). Additionally, this catalyst exhibited a high metal dispersion and optimal pore diameter from Co-chemisorption and XRD analysis. The minimum HDS (84%) and HDN (42%)

conversions were also obtained with the 2.5wt%Ni19wt%Mo/OCP_f catalyst because, of its low percentage dispersion (4.4%) coupled with it having the highest pore diameter (~13 nm). Even though this pore diameter was the highest amongst all the catalysts, it may not be the optimal. This is because, it would allow reactant molecules to access the catalytic sites without making maximum contact at the active sites for maximum activity results. Although the 5.0wt%Ni26wt%Mo/OCP_f catalyst had the lowest surface area of ~78 m^2/g and exhibited the lowest percentage metal dispersion of 3.8% and highest reducibility temperature, these properties did not have any negative impact on its corresponding HDS and HDN activities as the effect from its high hydrogen consumption intensity from TPR result in **Figure 6** outweighed or nullified the effect from the other characteristics. High hydrogen consumption also implied that the 5.0wt%Ni26wt%Mo/OCP_f catalyst had a high propensity of forming a Type II Ni-Mo-S with enhanced activity as confirmed by Yin et al., 2011 (Park et al., 1997; Yin et al., 2011).

CONCLUSION

In this study, seven catalysts with different combinations of Ni and Mo compositions were formulated, characterized, and used to hydrotreat light gas oil to ascertain how the OCP_f-supported catalysts contribute to the achievement of highest HDS and HDN activities. Characterization results from this study showed that although all the catalysts displayed mesoporous pore diameters ranging from 10–13 nm, the surface areas (<110 m^2/g) and pore volumes (~0.12 cm^3/g) of all catalysts were low. Additionally, TGA analysis confirmed that all catalysts formulated from an OCP_f by-product support material can attain high thermal stability with low weight loss (1%) within the hydrotreating operating temperatures (330–370°C) experimented. CO-chemisorption results concludes that high Ni composition of 5.0 wt% played a dominant role in decreasing crystallite sites and enhancing the percentage metal dispersion and CO uptake. TPR analysis indicates that for catalysts with similar metal-support-interaction their HDS and HDN activities can be high if they exhibit high hydrogen consumption intensities. In this regard, amongst all the catalysts under study, the 5.0wt%Ni19wt%Mo/OCP_f demonstrated the highest HDS and HDN activities of 90 and 50%, respectively with light gas oil at a hydrotreating operating pressure of 9.0 MPa, temperature of 370°C and LHSV of 2 h^{-1}. As evidence from XRD, CO chemisorption, and TPR results, the HDS and HDN catalytic activities were influenced by the presence of crystals such as MoO_3 and NiO in all the catalyst samples. At the highest operating temperature of 370°C, the effect of variation in metal loading compositions on HDS activities was not significant since some catalysts displayed similar HDS activities. However, in the case of the HDN activities apart from the 5.0wt%Ni26wt%Mo/OCP_f catalyst, a steady increase in activity occurred as the metal loading compositions on the OCP_f support increased. In situations, where physical separation of materials precedes catalyst formulation the particle cutoff size has an impact on HDS and HDN activities since finer materials are more likely to have better physiochemical characteristics suitable for the development of a hydrotreating catalyst. Use of a lower LHSV for sulfidation can also lead to an improvement in HDS and HDN activities. Outcome from this study demonstrates that the NiMo/OCP_f catalyst can be improved and used in catalysis for hydrotreating or other similar catalytic reactions.

DATA AVAILABILITY STATEMENT

The raw data supporting the conclusion of this article will be made available by the authors, without undue reservation.

AUTHOR CONTRIBUTIONS

EA designed and conducted all experiments, analyzed experimental results, wrote the draft of the manuscript and revised the final submission. AKD and JA approved the experimental plan, supervised the work, reviewed and modified the final submission. All authors listed have made a substantial, direct and intellectual contribution to the work and approve it for publication.

ACKNOWLEDGMENTS

The financial support from Syncrude, Canada Research Chair (CRC) Program, University of Saskatchewan, MITACS and Natural Sciences and Engineering Research Council of Canada (NSERC) are gratefully acknowledged.

REFERENCES

Afanasiev, P., and Bezverkhyy, I. (2007). Ternary Transition Metals Sulfides in Hydrotreating Catalysis. *Appl. Catal. A: Gen.* 322, 129–141. doi:10.1016/j.apcata.2007.01.015

Al-Dahhan, M. H., Wu, Y., and Dudukovic, M. P. (1995). Reproducible Technique for Packing Laboratory-Scale Trickle-Bed Reactors with a Mixture of Catalyst and Fines. *Ind. Eng. Chem. Res.* 34, 741–747. doi:10.1021/ie00042a005

Arora, N., and Sharma, N. N. (2014). Arc Discharge Synthesis of Carbon Nanotubes: Comprehensive Review. *Diamond Relat. Mater.* 50, 135–150. doi:10.1016/j.diamond.2014.10.001

Aryee, E., Dalai, A. K., and Adjaye, J. (2014). Functionalization and Characterization of Carbon Nanohorns (CNHs) for Hydrotreating of Gas Oils. *Top. Catal.* 57, 796–805. doi:10.1007/s11244-013-0236-6

Aryee, E., Essilfie-Dughan, J., Dalai, A. K., and Adjaye, J. (2021). Comparative Studies of Carbon Nanomaterial and γ-Alumina as Supports for the Ni-Mo Catalyst in Hydrotreating of Gas Oils. *Energy Fuels* 35, 6153–6166. doi:10.1021/acs.energyfuels.0c02394

Aryee, E. (2019).Hydrotreating of Gas Oils Using Ni-Mo Catalyst Supported on Carbon Nanohorns and Associated Carbon Materials. Doctor of Philosophy Thesis. University of Saskatchewan. Available at: http://hdl.handle.net/10388/12383.

Badoga, S., Sharma, R. V., Dalai, A. K., and Adjaye, J. (2014). Hydrotreating of Heavy Gas Oil on Mesoporous Zirconia Supported NiMo Catalyst with EDTA. *Fuel* 128, 30–38. doi:10.1016/j.fuel.2014.02.056

Bartholomew, C. H. (2001). Mechanisms of Catalyst Deactivation. *Appl. Catal. A: Gen.* 212, 17–60. doi:10.1016/s0926-860x(00)00843-7

Bekyarova, E., Kaneko, K., Kasuya, D., Murata, K., Yudasaka, M., and Iijima, S. (2002). Oxidation and Porosity Evaluation of Budlike Single-wall Carbon Nanohorn Aggregates. *Langmuir* 18, 4138–4141. doi:10.1021/la0117348

Botchwey, C., Dalai, A. K., and Adjaye, J. (2003). Product Selectivity during Hydrotreating and Mild Hydrocracking of Bitumen-Derived Gas Oil. *Energy Fuels* 17, 1372–1381. doi:10.1021/ef020214x

Brito, J. n. L., Laine, J., and Pratt, K. C. (1989). Temperature-Programmed Reduction of Ni-Mo Oxides. *J. Mater. Sci.* 24, 425–431. doi:10.1007/bf01107422

Byskov, L. S., Hammer, B., Nørskov, J. K., Clausen, B. S., and Topsøe, H. (1997). Sulfur Bonding in MoS_2 and Co-mo-S Structures. *Catal. Lett.* 47, 177–182. doi:10.1023/A:1019009105792

Calafat, A., Laine, J., López-Agudo, A., and Palacios, J. M. (1996). Effect of Surface Oxidation of the Support on the Thiophene Hydrodesulfurization Activity of Mo, Ni, and NiMo Catalysts Supported on Activated Carbon. *J. Catal.* 162, 20–30. doi:10.1006/jcat.1996.0256

Candia, R., Sørensen, O., Villadsen, J., Topsøe, N.-Y., Clausen, B. S., and Topsøe, H. (1984). Effect of Sulfiding Temperature on Activity and Structures of CO-MO/AL2O3 Catalysts. *Ii. Bull. Soc. Chim. Belges.* 93, 763–774. doi:10.1002/bscb.19840930818

Duchet, J., van Oers, E. M., de Beer, V. H. J., and Prins, R. (1983). Carbon-supported Sulfide Catalysts. *J. Catal.* 80, 386–402. doi:10.1016/0021-9517(83)90263-4

Ebbesen, T. W., and Ajayan, P. M. (1992). Large-scale Synthesis of Carbon Nanotubes. *Nature* 358, 220–222. doi:10.1038/358220a0

Falcao, E. H., and Wudl, F. (2007). Carbon Allotropes: beyond Graphite and diamond. *J. Chem. Technol. Biotechnol.* 82, 524–531. doi:10.1002/jctb.1693

Fogler, H. (2006). *Elements of Chemical Reaction Engineering*. 4th Edition. Upper Saddle River, NJ: Prentice Hall International Series.

Furimsky, E. (1998). Selection of Catalysts and Reactors for Hydroprocessing. *Appl. Catal. A: Gen.* 171, 177–206. doi:10.1016/S0926-860X(98)00086-6

Grimblot, J. (1998). Genesis, Architecture and Nature of Sites of Co(Ni)-MoS2 Supported Hydroprocessing Catalysts. *Catal. Today* 41, 111–128. doi:10.1016/S0920-5861(98)00042-X

Hurst, N. W., Gentry, S. J., Jones, A., and McNicol, B. D. (1982). Temperature Programmed Reduction. *Catal. Rev.* 24, 233–309. doi:10.1080/03602458208079654

Jarullah, A. T., Mujtaba, I. M., and Wood, A. S. (2012). Improving Fuel Quality by Whole Crude Oil Hydrotreating: A Kinetic Model for Hydrodeasphaltenization in a Trickle Bed Reactor. *Appl. Energ.* 94, 182–191. doi:10.1016/j.apenergy.2012.01.044

Kaluža, L., and Zdražil, M. (2001). Carbon-supported Mo Catalysts Prepared by a New Impregnation Method Using a MoO3/water Slurry: Saturated Loading, Hydrodesulfurization Activity and Promotion by Co. *Carbon* 39, 2023–2034. doi:10.1016/s0008-6223(01)00018-5

Karousis, N., Suarez-Martinez, I., Ewels, C. P., and Tagmatarchis, N. (2016). Structure, Properties, Functionalization, and Applications of Carbon Nanohorns. *Chem. Rev.* 116, 4850–4883. doi:10.1021/acs.chemrev.5b00611

Keidar, M., Shashurin, A., Li, J., Volotskova, O., Kundrapu, M., and Zhuang, T. S. (2011). Arc Plasma Synthesis of Carbon Nanostructures: where Is the Frontier. *J. Phys. D: Appl. Phys.* 44, 174006–174011. doi:10.1088/0022-3727/44/17/174006

Lam, E., and Luong, J. H. T. (2014). Carbon Materials as Catalyst Supports and Catalysts in the Transformation of Biomass to Fuels and Chemicals. *ACS Catal.* 4, 3393–3410. doi:10.1021/cs5008393

Laredo S, G. C., De los Reyes H, J. A., Luis Cano D, J., and Jesús Castillo M, J. (2001). Inhibition Effects of Nitrogen Compounds on the Hydrodesulfurization of Dibenzothiophene. *Appl. Catal. A: Gen.* 207, 103–112. doi:10.1016/S0926-860X(00)00620-7

Lebukhova, N. V., and Karpovich, N. F. (2008). Carbothermic Reduction of Copper, Nickel, and Cobalt Oxides and Molybdates. *Inorg. Mater.* 44, 890–893. doi:10.1134/s0020168508080207

Liu, F., Xu, S., Chi, Y., and Xue, D. (2011). A Novel Alumina-Activated Carbon Composite Supported NiMo Catalyst for Hydrodesulfurization of Dibenzothiophene. *Catal. Commun.* 12, 521–524. doi:10.1016/j.catcom.2010.11.018

López, C. R., and López, A. A. (2000). Effect of Water Extraction on the Surface Properties of Mo/Al_2O_3 and $NiMo/Al_2O_3$ Hydrotreating Catalysts. *Appl. Catal. A: Gen.* 202, 23–35. doi:10.1016/S0926-860X(00)00449-X

Lynch, J. (2003). *Physico-chemical Analysis of Industrial Catalysts - A Practical Guide to Characterization*. Paris: Editions TECHNIP, 1–309.

Mapiour, M., Sundaramurthy, V., Dalai, A. K., and Adjaye, J. (2010). Effects of the Operating Variables on Hydrotreating of Heavy Gas Oil: Experimental, Modeling, and Kinetic Studies. *Fuel* 89, 2536–2543. doi:10.1016/j.fuel.2010.02.024

Micromeritics ASAP (2020). Chemi Manual. Appendix C.

Mirabile Gattia, D., Vittori Antisari, M., Marazzi, R., Pilloni, L., Contini, V., Montone, A., et al. (2006). Arc-discharge Synthesis of Carbon Nanohorns and Multiwalled Carbon Nanotubes. *Materials Science Forum* 518, 23–28. doi:10.4028/www.scientific.net/msf.518.23

Ng, J., and Raitses, Y. (2014). Role of the Cathode deposit in the Carbon Arc for the Synthesis of Nanomaterials. *Carbon* 77, 80–88. doi:10.1016/j.carbon.2014.05.007

Park, Y.-C., Oh, E.-S., and Rhee, H.-K. (1997). Characterization and Catalytic Activity of WNiMo/Al2O3 Catalyst for Hydrodenitrogenation of Pyridine. *Ind. Eng. Chem. Res.* 36, 5083–5089. doi:10.1021/ie970386v

Prins, R., de Beer, V. H. J., and Somorjai, G. A. (1989). Structure and Function of the Catalyst and the Promoter in Co-mo Hydrodesulfurization Catalysts. *Catal. Rev.* 31, 1–41. doi:10.1080/01614948909351347

Qu, L., Zhang, W. P., Kooyman, P. J., and Prins, R. (2003). MAS NMR, TPR, and TEM Studies of the Interaction of NiMo with Alumina and Silica-Alumina Supports. *J. Catal.* 215, 7–13. doi:10.1016/s0021-9517(02)00181-1

Quanli, Z., Bing, Z., Jian, Y., Jiaxin, W., Jun, Z., Shengfu, J., et al. (2003). The Promotion of Nickel to Mo2C/Al2O3 Catalyst for the Partial Oxidation of Methane to Syngas. *New J. Chem.* 27, 1633–1638. doi:10.1039/b306485a

Rana, M. S., Torres-Mancera, P., and Ancheyta, J. (2020). *Experimental Methods for Evaluation of Hydrotreating Catalysts//Experimentation in Glass Reactors with Model Compounds*. 1st Edition, 11–45. doi:10.1002/9781119518037.ch2

Regalbuto, J. R., and Ha, J.-W. (1994). A Corrected Procedure and Consistent Interpretation for Temperature Programmed Reduction of Supported MoO3. *Catal. Lett.* 29, 189–207. doi:10.1007/bf00814265

Robinson, P. R., and Dolbear, G. E. (2006). "Hydrotreating and Hydrocracking: Fundamentals," in *Practical Advances in Petroleum Processing*. Editors C. S. Hsu and P. R. Robinson (New York, NY: Springer), 177–218. doi:10.1007/978-0-387-25789-1_7

Rodriquez-Reinoso, F. (1998). The Role of Carbon Materials in Heterogenous Catalysis. *Carbon* 36, 159–175. doi:10.1016/S0008-6223(97)00173-5

Saito, Y., Yoshikawa, T., Inagaki, M., Tomita, M., and Hayashi, T. (1993). Growth and Structure of Graphitic Tubules and Polyhedral Particles in Arc-Discharge. *Chem. Phys. Lett.* 204, 277–282. doi:10.1016/0009-2614(93)90009-P

Sano, Y., Choi, K., Korai, Y., and Mochida, I. (2004). Adsorptive Removal of Sulfur and Nitrogen Species from a Straight Run Gas Oil over Activated Carbons for its Deep Hydrodesulfurization. *Appl. Catal. B: Environ.* 49, 219–225. doi:10.1016/j.apcatb.2003.12.007

Satterfield, C. (1991). *Heterogeneous Catalysis in Industrial Practice*. 2nd Edition. New York: McGraw-Hill.

Scheffer, B., van Oers, E. M., Arnoldy, P., de Beer, V. H. J., and Moulijn, J. A. (1986). Sulfidability and HDS Activity of Co-Mo/Al2O3 Catalysts. *Appl. Catal.* 25, 303–311. doi:10.1016/S0166-9834(00)81248-8

Serp, P., Corrias, M., and Kalck, P. (2003). Carbon Nanotubes and Nanofibers in Catalysis. *Appl. Catal. A: Gen.* 253, 337–358. doi:10.1016/s0926-860x(03)00549-0

Sing, K., Everett, D., Haul, R., Moscou, L., Pierotti, R., Rouquerol, J., et al. (1985). Reporting Physisorption Data for Gas/solid Systems with Special Reference to the Determination of Surface Area and Porosity. *Pure Appl. Chem.* 57, 603–619. doi:10.1002/9783527610044.hetcat0065

Speight, J. G. (2000). *The Desulfurization of Heavy Oils and Residua*. 2nd Edition. New York: Marcel Dekker.

Spevack, P. A., and Mcintyre, N. S. (1992). Thermal Reduction of Molybdenum Trioxide. *J. Phys. Chem.* 96, 9029–9035. doi:10.1021/j100201a062

Tang, D., Sun, L., Zhou, J., Zhou, W., and Xie, S. (2005). Two Possible Emission Mechanisms Involved in the Arc Discharge Method of Carbon Nanotube Preparation. *Carbon* 43, 2812–2816. doi:10.1016/j.carbon.2005.05.034

Titirici, M.-M., and Antonietti, M. (2010). Chemistry and Materials Options of Sustainable Carbon Materials Made by Hydrothermal Carbonization. *Chem. Soc. Rev.* 39, 103–116. doi:10.1039/B819318P

Van Veen, J. A. R., Colijn, H. A., Hendriks, P. A. J. M., and van Welsenes, A. J. (1993). On the Formation of Type I and Type II NiMoS Phases in NiMo/Al2O3

Hydrotreating Catalysts and its Catalytic Implications. *Fuel Process. Techn.* 35, 137–157. doi:10.1016/0378-3820(93)90089-M

Vissers, J., Scheffer, B., de Beer, V., Moulijn, J., and Prins, R. (1987). Effect of the Support on the Structure of Mo-Based Hydrodesulfurization Catalysts: Activated Carbon versus Alumina*1. *J. Catal.* 105, 277–284. doi:10.1016/0021-9517(87)90058-3

Yeh, Y.-W., Raitses, Y., and Yao, N. (2016). Structural Variations of the Cathode deposit in the Carbon Arc. *Carbon* 105, 490–495. doi:10.1016/j.carbon.2016.04.074

Yin, H., Zhou, T., Liu, Y., Chai, Y., and Liu, C. (2011). NiMo/Al2O3 Catalyst Containing Nano-Sized Zeolite Y for Deep Hydrodesulfurization and Hydrodenitrogenation of Diesel. *J. Nat. Gas Chem.* 20, 441–448. doi:10.1016/s1003-9953(10)60204-6

Zhang, D., Ye, K., Yao, Y., Liang, F., Qu, T., Ma, W., et al. (2019). Controllable Synthesis of Carbon Nanomaterials by Direct Current Arc Discharge from the Inner wall of the Chamber. *Carbon* 142, 278–284. doi:10.1016/j.carbon.2018.10.062

Conflict of Interest: Author JA was employed by company Syncrude Edmonton Research Centre.

The remaining authors declare that the research was conducted in the absence of any commercial or financial relationships that could be construed as a potential conflict of interest.

Publisher's Note: All claims expressed in this article are solely those of the authors and do not necessarily represent those of their affiliated organizations, or those of the publisher, the editors and the reviewers. Any product that may be evaluated in this article, or claim that may be made by its manufacturer, is not guaranteed or endorsed by the publisher.